A Fast Way to Visualize the Brain Surface With Volume Rendering of MRI Data

Sumiaki Matsumoto, Reinin Asato, and Junji Konishi

The preprocessing of 3-dimensional (3D) MRI data constitutes a bottleneck in the process of visualizing the brain surface with volume rendering. As a fast way to achieve this preprocessing, the authors propose a simple pipeline based on an algorithm of seed-growing type, for approximate segmentation of the intradural space in T1-weighted 3D MRI data. Except for the setting of a seed and four parameters, this pipeline proceeds in an unsupervised manner; no interactive intermediate step is involved. It was tested with 15 datasets from normal adults. The result was reproducible in that as long as the seed was located within the cerebral white matter, identical segmentation was achieved for each dataset. Although the pipeline ran with gross segmentation error along the floor of the cranial cavity, it performed well along the cranial vault so that subsequent volume rendering permitted the observation of the sulco-gyral pattern over cerebral convexities. Use of this pipeline followed by volume rendering is a handy approach to the visualization of the brain surface from 3D MRI data.

KEY WORDS: magnetic resonance imaging, segmentation, intradural space, volume rendering, visualization, brain surface.

VOLUME RENDERING is a relatively new approach to visualization of 3-dimensional (3D) data, but since its inception, one of its major application fields has been medical imaging.[1] The power of volume rendering as a tool for creating brain surface views from MRI data has long been recognized.[2] On the other hand, because of its computational burden, volume rendering has not been used as widely as traditional surface rendering. However, the situation is changing; the current trend toward larger memories and faster processors at lower cost is making volume rendering accessible to an increasing number of computer users.

Volume rendering does not require precise segmentation of the object of interest. When the target of visualization is the brain surface, the preprocessing of 3D MRI data only involves removal of voxels that are neither the brain nor the cerebrospinal fluid (CSF). Here it is not necessary to segment the intradural space exactly; pure CSF voxels may be removed to a variable extent without affecting the quality of rendering. In contrast, if brain surface views are to be created with surface rendering, brain volume must be segmented accurately; any segmentation error is carried through to subsequent rendering. However, accurate segmentation of brain volume is difficult because a typical 3D MRI dataset usually is single-valued (T1-weighted in most cases) and precludes use of the pattern recognition approach in multidimensional feature space.[3] Although various solutions to this problem have been proposed,[4-9] they have one or more of the following drawbacks: (1) the possibility of inter- and intra-operator variability,[4-7] (2) the necessity of continuous operator supervision and intervention,[5,6] and (3) the assumption of prior correction of intensity nonuniformity over the imaging volume.[7-9] Considering the relative ease of preprocessing, volume rendering is more attractive as a technique for visualizing the brain surface from 3D MRI data.

Nevertheless, the preprocessing of 3D MRI data for volume rendering constitutes a bottleneck in the process of visualization of the brain surface. The methods for this step used in previous works involve continuous supervision by the operator, and thus are laborious and time-consuming.[2,10] With this knowledge, we developed a simple and fast pipeline that prepares T1-weighted 3D MRI data for the creation of brain surface views with volume rendering. Below it is described in detail, and an evaluation of its performance is presented.

METHODS

Overview of the Pipeline

For a given T1-weighted 3D MRI dataset, the pipeline produces a mask that approximately covers the intradural space. It exploits one of the basic properties of T1-weighted MRI data: if the data is examined locally and no artifact is present, signal intensity decreases in the order of white matter, grey matter, and CSF.

From the Department of Nuclear Medicine and Diagnostic Imaging, Faculty of Medicine, Kyoto University, Kyoto, Japan.

Address reprint requests to Sumiaki Matsumoto, MD, Department of Nuclear Medicine and Diagnostic Imaging, Faculty of Medicine, Kyoto University, 54 Shogoin-kawahara-cho, Sakyo-ku, Kyoto 606-8507, Japan.

0897-1889/99/1204-0005$10.00/0

The pipeline consists of three steps: noise reduction, region growing from a seed, and postprocessing. As will be detailed herein, the pipeline has 4 parameters to adjust in advance, but does not demand operator interaction except for the setting of a seed voxel.

Noise Reduction

The goal of this preparatory step is to make the data less noisy without blurring the edges. Thus, anisotropic diffusion filtering,[11] is employed. The formula of anisotropic diffusion filtering used here is

$$I(t + \Delta t) = I(t) + \Delta t^* \Sigma(\exp(-(\nabla I/\kappa)^2)^*\nabla I)$$

where t is the process ordering parameter, I is the signal intensity at a voxel, and ∇I is the local intensity gradient. The summation (Σ) applies to the neighborhood of a voxel, and the parameter κ must be adjusted based on noise in the data. In our implementation, the system of 6-connected neighborhood is adopted, and the number of iteration is fixed at 2.

Region Growing From a Seed

This step is central to the pipeline and consists of 2 phases. The algorithm below is common to both phases. Note that any 3D mask can be represented equivalently by the corresponding set of voxels.

M_{in} = the input set of voxels

M_{out} = the output set of voxels

M, N = temporary sets

$\{\}$ = the empty set

$S(v)$ = signal intensity of a voxel v

$\{v\}$ = the set whose sole member is v

1. $M = M_{in}$
2. $N = \{\}$
3. for every voxel v in M
   3.1 for every voxel v' in the 6-connected neighborhood of v
   if ($v' \notin M$ and $v' \notin N$) and ($S(v')$ fulfills a criterion) then $N = N \cup \{v'\}$
4. if ($N \neq \{\}$), then $M = M \cup N$, and go to 2; else $M_{out} = M$

When M_{in} is comprised of a single voxel, the algorithm can be called seed-growing. In the first phase, this mode of operation is employed. Namely, a seed voxel is selected interactively by the operator in the cerebral white matter. And the explicit form of the criterion in step 3.1 is:

$$|S(v') - S(v)| \leqq D_1$$

(D_1 = a non-negative constant)

Note that this algorithm is equivalent to that described by Cline et al[7] when the criterion becomes

$$Th \leqq S(v') \quad (Th = \text{a positive constant})$$

When D_1 is sufficiently small, the first phase yields a mask that covers a volume within which signal intensity varies smoothly. Because the seed voxel is placed in the cerebral white matter, the resulting mask extends into every region of the brain mainly along the white matter, but does not include CSF owing to the contrast between the brain and CSF.

In the second phase, M_{out} of the first phase is used as M_{in}. This time the criterion is

$$S(v') - S(v) \leqq D_2$$

(D_2 = a non-negative constant)

If D_2 is zero, region-growing occurs only where signal intensity decreases in the direction of region-growing. Because signal intensity decreases locally in the order of white matter, grey matter, and CSF, the input mask (the output of the first phase) is expected to grow until the resulting mask covers the entire brain while minimally including non-brain and non-CSF voxels.

In practice, we use the following criteria for the second phase:

$$S(v') - S(v) \leqq D_2$$

$$S(v') \geqq T_{cutoff}$$

Here D_2 is not zero but takes a small positive value to accommodate the effect of residual noise. T_{cutoff} is set so as to prevent the mask to incorporate voxels whose signal intensities are at background level, and thereby to reduce computation time.

Postprocessing

In general, many small "holes" are present in the mask at this point (Fig 1), but they can be removed easily. First, the mask is converted to a stack of 2-dimensional (2D) masks. We can assume that the corner- and border-pixels are zero in each 2D mask. Then the "holes" correspond to the zeros in each

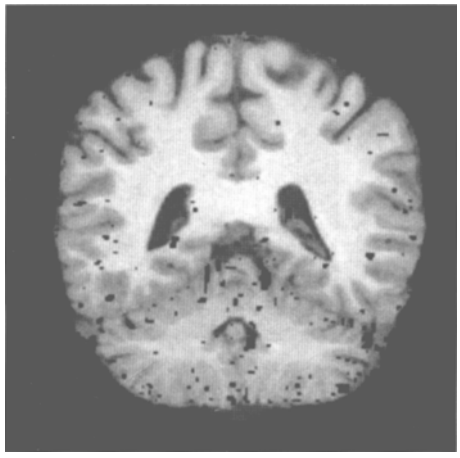

Fig 1. An intermediate mask after the second step of the pipeline with many "holes." This example is from the data used in the next figure, and is shown in the same coronal plane as in the bottom row of Fig 2.

2D mask that are isolated from the zeros along the corners and borders, and can be eliminated by applying slice-by-slice the following algorithm, which has the same structure as the previous one. Again, note that any 2D mask has the equivalent set of pixels.

M_{all} = the set of all pixels in a given slice

M_{in} = the input set of pixels

M_{out} = the output set of pixels

M, N = temporary sets

$\overline{M}$ = the complement of M defined by $M \cup \overline{M}$

$= M_{all}$ and $M \cap \overline{M} = \{\}$

q = one of the corner pixels

1. $M = \{q\}$
2. $N = \{\}$
3. for every pixel p in M
   3.1 for every pixel p' in the 4-connected neighborhood of p
   if ($p' \notin M$ and $p' \notin N$ and $p' \in \overline{M}_{in}$) then $N = N \cup \{p'\}$
4. if ($N \neq \{\}$), then $M = M \cup N$, and go to 2; else $M_{out} = \overline{M}$

The 3D extension of this algorithm is straightforward, but not used here because some of "holes" are not isolated in three dimensions.

Experiment

Fifteen datasets of healthy volunteers (age range, 20 to 50 years) were obtained with a 1.5-T unit (Horizon; General Electric Medical Systems, Milwaukee, WI). The sequence used was 3D spoiled-gradient recalled echo (3D-SPGR) in the coronal orientation, with the following parameters: slice thickness = 1.5 mm, number of slices = 124, TE = 3 ms, TR = 30 ms, flip angle = 30°, acquisition matrix = 192 (phase) × 256 (frequency), NEX = 1, and FOV = 20 cm.

These datasets were subjected to the proposed pipeline that was implemented on a workstation (Ultra1; Sun Microsystems, Inc, Mountain View, CA) using C programming language and MATLAB (The MathWorks Inc, Natick, MA). On an empirical basis, the 4 parameters were fixedly linked to the standard deviation of noise (Nstd) that was determined in the background region[12]: κ, D_1, D_2, and T_{cutoff} were set (respectively) to 2 * Nstd, 0.3 * Nstd, 0.3 * Nstd, and 5 * Nstd. Because the result can depend on the location of the seed, the region-growing step was repeated 20 times for each dataset, with the seed being chosen randomly each time. Each mask produced by the pipeline was multiplied by the original 3D data, and volume-rendered. Volume rendering was done using AVS (Advanced Visual Systems Inc, Waltham, MA), and views from 4 angles (right, left, superior, and inferior) were assessed by visual inspection.

RESULTS

Figure 2 illustrates how the pipeline proceeds. The processing time for one dataset was about 10 minutes. The pipeline reached the identical segmentation for each dataset, irrespective of the location of the seed. The final mask was confined within the intradural space for the most part, but partially included the dural venous sinuses. It was commonly observed that, owing to the blood flow, the voxels thus included demonstrated signal intensities close to those of brain voxels, leading to the obscuration of the brain surface after volume rendering. Because of their anatomic locations, however, these voxels in the dural venous sinuses interfered little with the observation of the cerebral sulco-gyral pattern. Problematic was the presence of many brain voxels near the brain surface that failed to be included in the mask. Grossly apparent

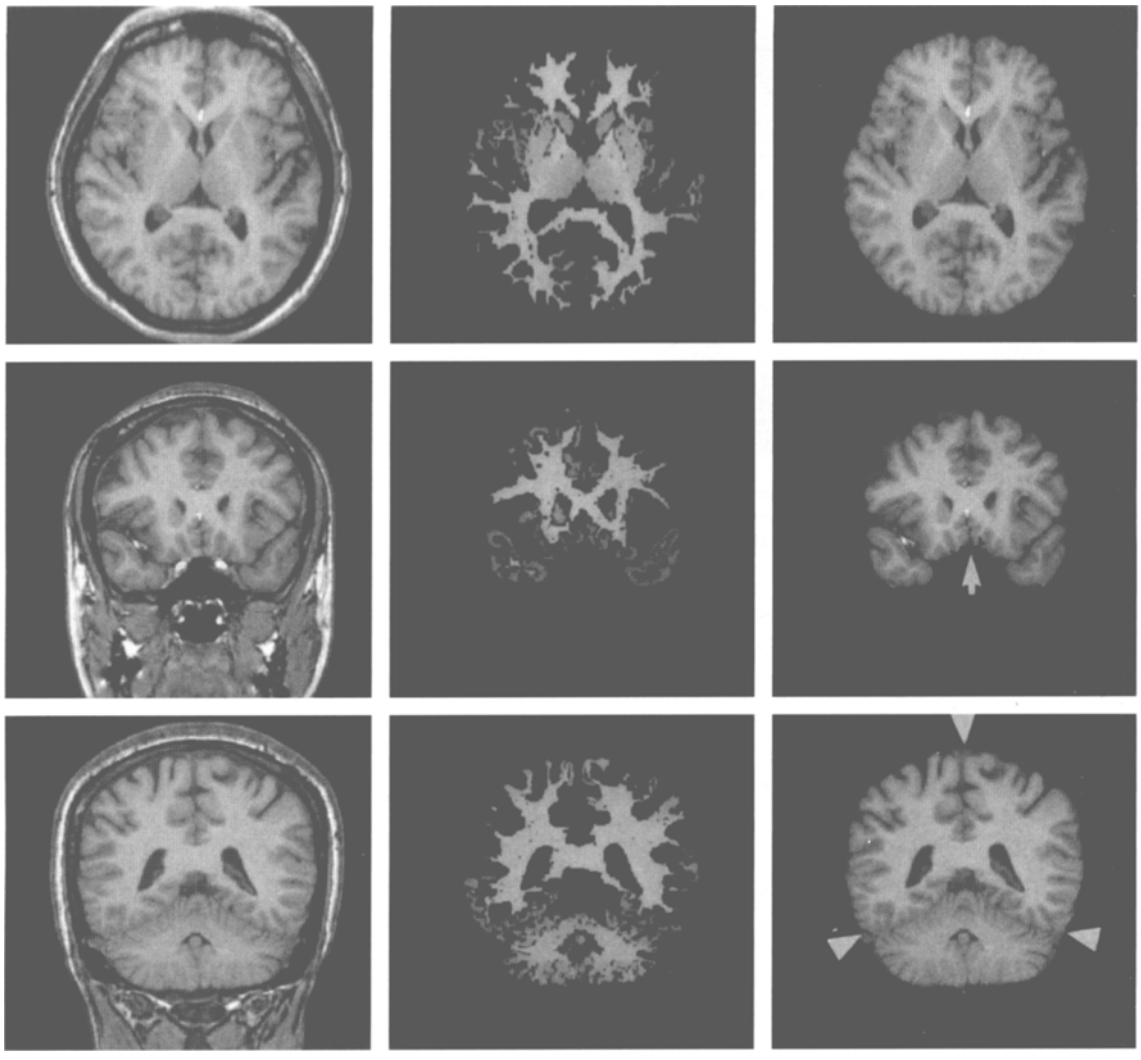

Fig 2. Progression of the pipeline as seen in an axial plane (top row) and coronal planes (middle and bottom rows). Left column: Data filtered with anisotropic diffusion; Middle column: intermediate mask after the first phase of the second step, multiplied by unsegmented data; Right column: final mask multiplied by unsegmented data. The segmentation is as good as intended for the most part, but imperfect at the dural venous sinuses (arrowheads) and along the floor of the cranial cavity (arrow).

imperfections in volume-rendered views resulted from this error. Using a specially developed software tool, the voxels contributing to the error were identified interactively, and the number of these voxels was counted. The counting was done separately along the following subdivisions of the inner surface of the cranial cavity: (1) the anterior and middle cranial fossae, (2) the posterior cranial fossa, and (3) along the cranial vault. Table 1 shows elementary statistics of the error. On average, the error was 2.87 cm^3, with 88.5% occurring in the anterior and middle cranial fossae. It was obvious that the majority of error was caused by artifacts in the vicinity of the paranasal sinuses or mastoid air cells. The amount of error along the cranial vault was negligible. Accordingly, in all datasets, error was most apparent on the volume-rendered inferior view; the other three views had quality sufficient

Table 1. Volume of Brain Voxels That the Pipeline Failed to Include

Anterior and Middle Cranial Fossae	Posterior Fossa	Cranial Vault	Total
2.54 ± 0.38	0.25 ± 0.10	0.08 ± 0.07	2.87 ± 0.44
88.5	8.7	2.8	100

NOTE. In the top row, values are expressed in cm^3 as mean ± standard deviation. In the bottom row, mean values are expressed as a percentage of the total.

for depicting the sulco-gyral pattern over the cerebral convexities. The sites of error in the posterior cranial fossa were not salient on volume-rendered views. Figure 3 shows examples of the brain surface views obtained.

DISCUSSION

The presented pipeline is built on the algorithm of seed-growing type, and thus is easy to implement and fast to execute. Furthermore, because its central step is steered by the comparison of signal intensities of neighboring voxels, the pipeline is immune to signal intensity variation of low spatial frequency. Although it is commonly held that robust segmentation is difficult to obtain with the algorithm of seed-growing type,[13] our results show that this is not necessarily the case, especially when the apparent signal-to-noise ratio of the data is increased by appropriate filtering such as anisotropic diffusion.

The utmost merit of this pipeline is that it needs no operator interaction in the middle of processing. Before the pipeline begins, the operator must tune the 4 parameters (κ, D_1, D_2, and T_{cutoff}) and supply the seed. But the processing itself proceeds automatically. Because the location of the seed does not affect the course of processing, as long as it is in the cerebral white matter, the final segmentation for a particular dataset is determined solely by the parameter tuning and is reproducible. In our experience, any dataset acquired with the same imaging parameters can be processed stably with the same tuning. Therefore, after the pipeline's parameters are appropriately set, unsupervised processing of multiple datasets is possible once the seed voxel is selected for each dataset.

The pipeline assumes that white matter, grey matter, and CSF show the signal intensities decreasing in this order. As a consequence of this assumption, it has the following obvious limitations: (1) it fails where data are corrupted by artifacts, and (2) it is not suited to data from patients with gross brain pathology. The first limitation is manifested by the pipeline's lowered performance along the floor of the cranial cavity, where a sudden change in

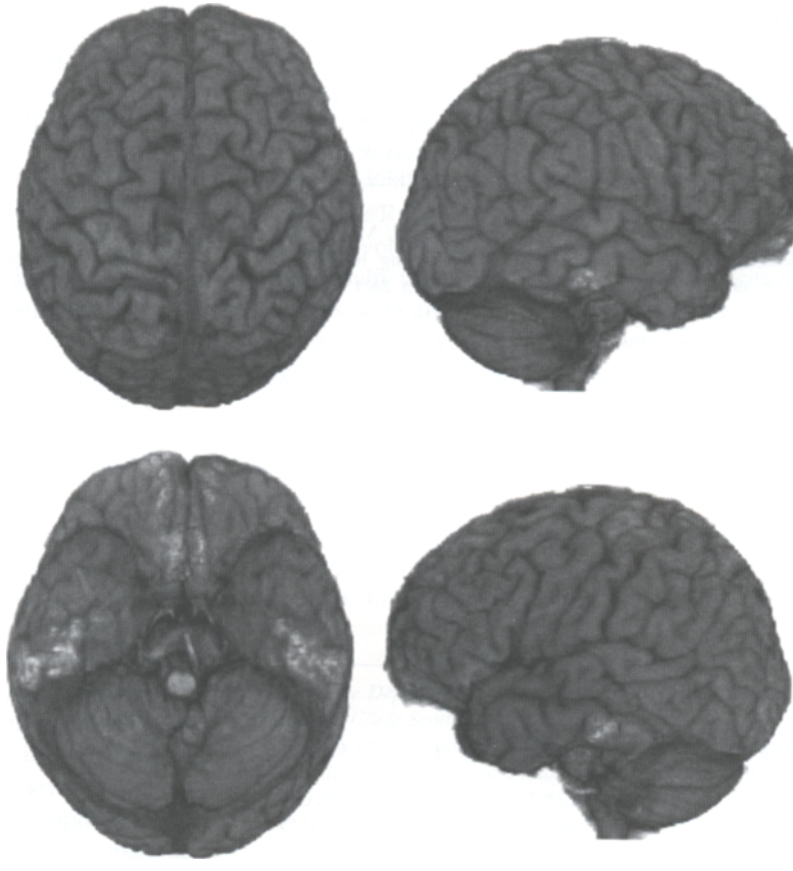

Fig 3. Typical volume-rendered brain surface views. The inferior surfaces of the frontal and temporal lobes appear partly effaced because of segmentation error. The unsharp appearance of the cerebral longitudinal fissure on the superior view is caused by partial inclusion of the superior sagittal sinus. The overall sulco-gyral pattern of the cerebral convexities is well visualized.

magnetic susceptibility at the air-bone interfaces gives rise to irreparable artifacts. This drawback is insignificant if one is concerned only with visualization of the cerebral convexities. The second limitation detracts from the general utility of the pipeline. However, recent literature indicates that, as the acquisition of 3D MRI data of the brain becomes a common practice, there is renewed interest in developmental variability of the human cerebral sulco-gyral pattern.[14-17] The proposed pipeline should be helpful for further MRI-based research on this subject, especially if the number of datasets to be processed is large.

To summarize, we have presented a simple and fast pipeline to approximately segment the intradural space in T1-weighted 3D MRI data in a reproducible and virtually unsupervised manner. The use of this pipeline, followed by volume rendering, is a handy way to visualize the brain surface from 3D MRI data.

REFERENCES

1. Frenkel KA: Volume rendering. Comm ACM 32:426-435, 1989

2. Levin DN, Hu X, Tan KK, et al: Surface of the brain: Three-dimensional MR images created with volume rendering. Radiology 171:277-280, 1989

3. Bezdek JC, Hall LO, Clarke LP: Review of MR image segmentation techniques using pattern recognition. Med Phys 20:1033-1048, 1993

4. Joliot M, Mazoyer BM: Three-dimensional segmentation and interpolation of magnetic resonance brain images. IEEE Trans Med Imaging 12:269-277, 1993

5. Filipek PA, Kennedy DN, Caviness VS, et al: Magnetic resonance imaging–based brain morphometry: Development and application to normal subjects. Ann Neurol 25:61-67, 1989

6. Bomans M, Höhne KH, Tiede U, et al: 3-D segmentation of MR images of the head for 3-D display. IEEE Trans Med Imaging 9:177-183, 1990

7. Cline HE, Dumoulin CL, Hart HR, et al: 3D reconstruction of the brain from magnetic resonance images using a connectivity algorithm. Magn Reson Imaging 5:345-352, 1987

8. Brummer ME, Mersereau RM, Eisner RL, et al: Automatic detection of brain contours in MRI data sets. IEEE Trans Med Imaging 12:153-166, 1993

9. Snell JW, Merickel MB, Ortega JM, et al: Model-based boundary estimation of complex objects using hierarchical active surface templates. Pattern Recognition 28:1599-1609, 1995

10. Toh MY, Falk RB, Main JS: Interactive brain atlas with the visible human project data: Development methods and techniques. Radiographics 16:1201-1206, 1996

11. Gerig G, Kübler O, Kikinis R, et al: Nonlinear anisotropic filtering of MRI data. IEEE Trans Med Imaging 11:221-232, 1992

12. Kaufman L, Kramer DM, Crooks LE, et al: Measuring signal-to-noise ratios in MR imaging. Radiology 173:265-267, 1989

13. Clarke LP, Velthuizen RP, Camacho MA, et al: MRI segmentation: Methods and applications. Magn Reson Imaging 13:343-368, 1995

14. Kikinis R, Shenton ME, Gerig G, et al: Temporal lobe sulco-gyral pattern anomalies in schizophrenia: an in vivo MR three-dimensional surface rendering study. Neurosci Lett 182:7-12, 1994

15. Sisodiya SM, Stevens JM, Fish DR, et al: The demonstration of gyral abnormalities in patients with cryptogenic partial epilepsy using three-dimensional MRI. Arch Neurol 53:28-34, 1996

16. Bartley AJ, Jones DW, Weinberger DR: Genetic variability of human brain size and cortical gyral patterns. Brain 120:257-269, 1997

17. Biondi A, Nogueira H, Dormont D, et al: Are the brains of monozygotic twins similar? A three-dimensional MR study. Am J Neuroradiol 19:1361-1367, 1998